European Radiology (2020) 30:2324–2333
https://doi.org/10.1007/s00330-019-06621-x

GASTROINTESTINAL

Dual-energy CT–based deep learning radiomics can improve lymph node metastasis risk prediction for gastric cancer

Jing Li[1,2] · Di Dong[3,4] · Mengjie Fang[3,4] · Rui Wang[2] · Jie Tian[3,5,6] · Hailiang Li[1] · Jianbo Gao[2]

Received: 30 July 2019 / Revised: 15 November 2019 / Accepted: 12 December 2019 / Published online: 17 January 2020

Abstract

Objectives To build a dual-energy CT (DECT)–based deep learning radiomics nomogram for lymph node metastasis (LNM) prediction in gastric cancer.

Materials and methods Preoperative DECT images were retrospectively collected from 204 pathologically confirmed cases of gastric adenocarcinoma (mean age, 58 years; range, 28–81 years; 157 men [mean age, 60 years; range, 28–81 years] and 47 women [mean age, 54 years; range, 28–79 years]) between November 2011 and October 2018, They were divided into training ($n = 136$) and test ($n = 68$) sets. Radiomics features were extracted from monochromatic images at arterial phase (AP) and venous phase (VP). Clinical information, CT parameters, and follow-up data were collected. A radiomics nomogram for LNM prediction was built using deep learning approach and evaluated in test set using ROC analysis. Its prognostic performance was determined with Harrell's concordance index (C-index) based on patients' outcomes.

Results The dual-energy CT radiomics signature was associated with LNM in two sets (Mann-Whitney U test, $p < 0.001$) and an achieved area under the ROC curve (AUC) of 0.71 for AP and 0.76 for VP in test set. The nomogram incorporated the two radiomics signatures and CT-reported lymph node status exhibited AUCs of 0.84 in the training set and 0.82 in the test set. The C-indices of the nomogram for progression-free survival and overall survival prediction were 0.64 ($p = 0.004$) and 0.67 ($p = 0.002$).

Conclusion The DECT-based deep learning radiomics nomogram showed good performance in predicting LNM in gastric cancer. Furthermore, it was significantly associated with patients' prognosis.

Key Points

- *This study investigated the value of deep learning dual-energy CT–based radiomics in predicting lymph node metastasis in gastric cancer.*
- *The dual-energy CT–based radiomics nomogram outweighed the single-energy model and the clinical model.*
- *The nomogram also exhibited a significant prognostic ability for patient survival and enriched radiomics studies.*

Keywords Gastric cancer · Tomography, X-ray computed · Lymph node · Radiomics · Deep learning

Jing Li and Di Dong contributed equally to this work.

Electronic supplementary material The online version of this article (https://doi.org/10.1007/s00330-019-06621-x) contains supplementary material, which is available to authorized users.

✉ Jianbo Gao
gaojianbo_cancer@163.com

[1] Department of Radiology, the Affiliated Cancer Hospital of Zhengzhou University (Henan Cancer Hospital), Zhengzhou 450008, Henan, China

[2] Department of Radiology, the First Affiliated Hospital of Zhengzhou University, No. 1, East Jianshe Road, Zhengzhou 450052, Henan, China

[3] CAS Key Laboratory of Molecular Imaging, Institute of Automation, Chinese Academy of Sciences, Beijing 100190, China

[4] University of Chinese Academy of Sciences, Beijing 100049, China

[5] Engineering Research Center of Molecular and Neuro Imaging of Ministry of Education, School of Life Science and Technology, Xidian University, Xi'an 710126, Shaanxi, China

[6] Beijing Advanced Innovation Center for Big Data-Based Precision Medicine, School of Medicine, Beihang University, Beijing 100191, China

Abbreviations

AP	Arterial phase
AUC	Area under the receiver operating characteristic curve
CI	Confidence interval
GC	Gastric cancer
GSI	Gemstone spectral imaging
IC	Iodine concentration
LNM	Lymph node metastasis
MD	Material deposition
OS	Overall survival
PFS	Progression-free survival
VP	Venous phase

Introduction

Gastric cancer (GC) ranks as the fifth among all cancers and is the third leading cause of cancer-related mortality worldwide [1, 2]. Approximately 70% cases occur in Asia and more than half in China alone [3, 4]. N staging is crucial to select treatment options (endoscopy, surgery, neoadjuvant chemotherapy) [5–8] and helps prognosis prediction [9, 10]. CT is recommended as the first-line imaging technique for the detection of lymph node metastasis (LNM) by the National Comprehensive Cancer Network [11, 12], but its overall accuracy (around 60%) is disappointing [13–15].

Radiomics is an emerging approach that converts medical images to mineable data and generates thousands of quantitative features. This approach improves the performance in diagnosis and prognosis of cancer patients [16–18], which in turn helps in the clinical decision-making [19]. Notably, the association of radiomics signature with clinical features may improve the predictive accuracy of LNM in cancers [20–22]. Until now, most CT-based radiomics analyses have typically used one phase-enhanced image with single-energy scan mode. In terms of GC, CT has been used to extract a series of prognosis-related radiomics features [23] and was able to provide information for occult peritoneal metastasis prediction [24, 25]. Although previous studies proved dual-energy CT's ability to quantify response to neoadjuvant chemotherapy and the iodine concentration (IC) is an independent predictor for LNM in GC [26, 27], dual-energy CT–based radiomics for the prediction of LNM in GC have not yet to be reported. Meanwhile, the advanced deep learning method has become the mainstream approach for radiomics analyses based on big data medical imaging [28, 29]. Theoretically, the combination of dual-energy CT and deep learning methodology may potentially improve the predictive performance of radiomics nomogram.

The aim of this study was to build a dual-energy CT–based deep learning radiomics nomogram for the prediction of LNM and prognosis in patients with GC.

Materials and methods

Patients

Ethical approval was obtained from our institutional review board, but waiver of informed consent was required due to the retrospective nature of this study. A total 204 patients with pathologically confirmed gastric adenocarcinoma were recruited from November 2011 to October 2018. The inclusion and exclusion criteria are listed in Supplemental Material. Flow diagram for the patient selection is presented in Fig. 1. Computer-generated random numbers were adopted to divide patients into a training set ($n = 136$; 72.06% males; mean age, 58.98 ± 11.65 years; rang, 28–81 years) and a test set ($n = 68$; 72.06% males; mean age, 58.54 ± 10.79 years; range, 28–74 years).

Follow-up

Abdominal CT data of 133 patients were successfully collected between January 1st 2012 and December 31th 2018. Over a mean follow-up period of 32 months, 22 patients died and 30 showed progression. Both progression-free survival (PFS) and overall survival (OS) were measured from the first day of preoperative CT scan until the date of events (death for OS; death, metastasis and recurrence for PFS). The mean OS was 24.0 months, range of 4.0–72.0 months. The mean PFS was 18.2 months, range of 1.5–61.5 months. Patients were defined as the censored data if they did not achieve the events.

CT protocol

CT scans were performed using two versions of dual-energy CT in gemstone spectral imaging (GSI) mode (first or second generation Discovery CT750 HD scanner; GE Healthcare). The CT scans, covering the entire stomach region, were acquired with breath-hold with the patient head first supine in all of the phases. For enhanced CT scan, patients were infused 1.5 ml/kg of iodine (Ultravist 370, Bayer Schering Pharma) with a pump injector (Urich REF XD 2060-Touch, Ulrich Medical) at a rate of 3.0 ml/s into an antecubital vein. Arterial phase (AP) and venous phase (VP) contrast-enhanced CT images were performed after a 30 s and 70 s delay. The details on patient preparation and CT acquisition parameters were described in Supplemental Material.

Image interpretation and tumor segmentation

A radiologist with 12 years of experience in gastrointestinal radiology interpreted the dual phasic enhanced CT images and analyzed the iodine-water MD images by using GSI viewer software on dual-energy CT platform, as well as implemented tumor segmentation with ITK-SNAP version 3.6.0 software. The details were in Supplemental Material.

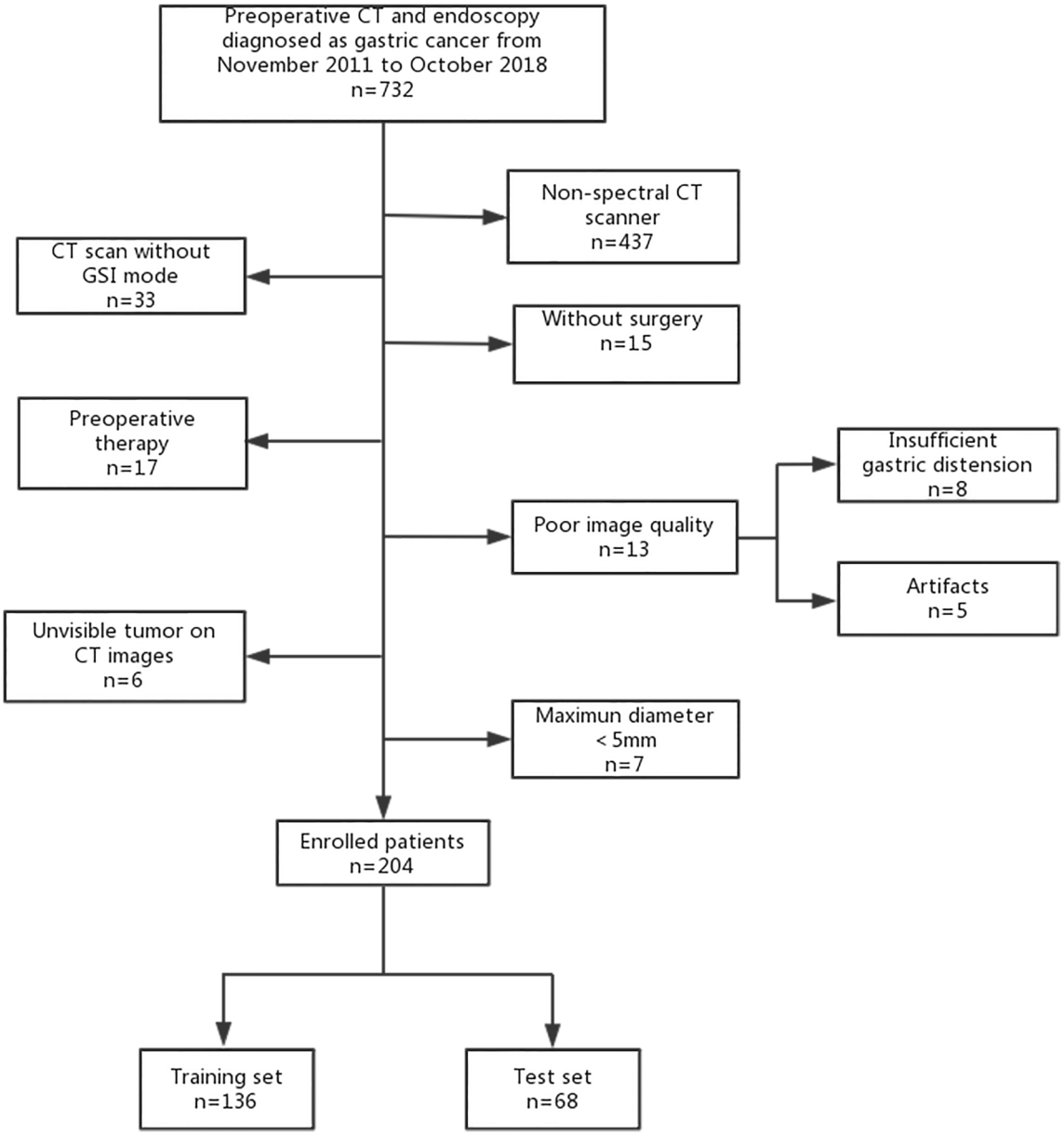

Fig. 1 Flow chart of patient selection process

Radiomics feature extraction

To quantify the tumor phenotypes, both deep learning features and handcrafted features were extracted. A total of 136 deep learning features and 391 handcrafted features were extracted from 40-, 65-, and 100-keV images for each CT phase. Based on the training set, two deep convolutional neural networks (DCNNs) were constructed and trained to extract the deep learning features in the two groups of ROIs. The details on the architecture and implementation of the constructed DCNNs and the feature extraction pipeline were described in Supplemental Material.

Feature selection and radiomics signature construction

The following processes were implemented to construct two radiomics signatures (i.e., the AP CT signature and the VP CT signature) to reflect the phenotypic characteristics of tumors.

Firstly, intra-class correlation coefficient (ICC) was calculated on the re-segmentation data to estimate the reproducibility of features. Only the stable features with ICC > 0.75 were reserved. Secondly, the features were divided into different groups, where each pair of features yielded a Pearson correlation coefficient of greater than 0.8. To build these feature groups, we examined the features in order of their

significances. We incorporated each feature into the group whose internal features correlated highly with it, or constructed a new group if it could not be incorporated into any existing group. Then, the most predictive feature (i.e., with the most significant p value) in each group was selected to obtain a stable and non-redundant candidate feature sets. For signature construction, four different models were compared: artificial neural network (ANN), k nearest neighbors (KNN), random forest (RF), and support vector machine (SVM). The best performing model as well as its final input features and optimized hype-parameters (i.e., the number of hidden neurons and the activation function in ANN, the number of neighbors and the distance metric in KNN, the minimum sample number required for a leaf node and the number of trees in RF, the penalty parameter, and the kernel coefficient in SVM) were obtained through multiple five-fold cross-validation applied on the training set.

Development of radiomics nomogram and comparative models

The chi-square test or Fisher's exact test was used to compare the differences in categorical variables between two groups, while the Mann-Whitney U test or independent t test was applied for continuous variables. The normality of the distribution of continuous variables was evaluated with the Shapiro test. A two-sided p value of < 0.05 was used as the criterion to indicate a statistically significant difference. In addition, multivariable logistic regression analysis with backward stepwise selection was performed to screen out key factors for LNM prediction. Akaike's information criterion (AIC) was used as the selection criterion. Then, a quantitative model was constructed using the regression coefficients and visualized as a radiomics nomogram (Fig. 2).

The above processes were also implemented to build a clinical model based on the clinical characteristics to simulate the clinical situation and to build a single-energy model combining the clinical characteristics with two single-energy (65 keV) signatures to explore the beneficial effect of the additional spectral information.

Statistical analysis

Receiver operating characteristic (ROC) curves were used to determine the predictive abilities of the involved models, while the DeLong test was used to compare different ROCs. The area under the curve (AUC) and 95% confidence interval (CI) were calculated. Quantitative performance of radiomics nomogram was assessed by calculating its accuracy. The calibration of the nomogram was evaluated by calibration curves using the Hosmer-Lemeshow test. Additionally, net reclassification index (NRI) was calculated to quantify the improvement in discrimination performance. To assess the reproducibility of our results, we randomly divided the patients into training set or test set five times. Subsequently, the nomogram was re-constructed and validated repeatedly.

To investigate the prognostic potential of radiomics nomogram, its association with patients' clinical outcomes (i.e., PFS and OS) was analyzed using univariable Cox regression model and Harrell's concordance index (C-index).

The software and the packages used for modeling and statistical analysis in this study are listed in Supplemental Material.

Results

Demographic and clinical characteristics of patients with GC

Demographic data, IC values and clinical features in two sets are listed in Table 1. Tumor thickness, nICVP, and CT-reported LN differed significantly between LNM-negative group and LNM-positive group in the training set ($p < 0.05$). No significant difference was observed between the two sets, in terms of age, sex, tumor location, and LNM prevalence.

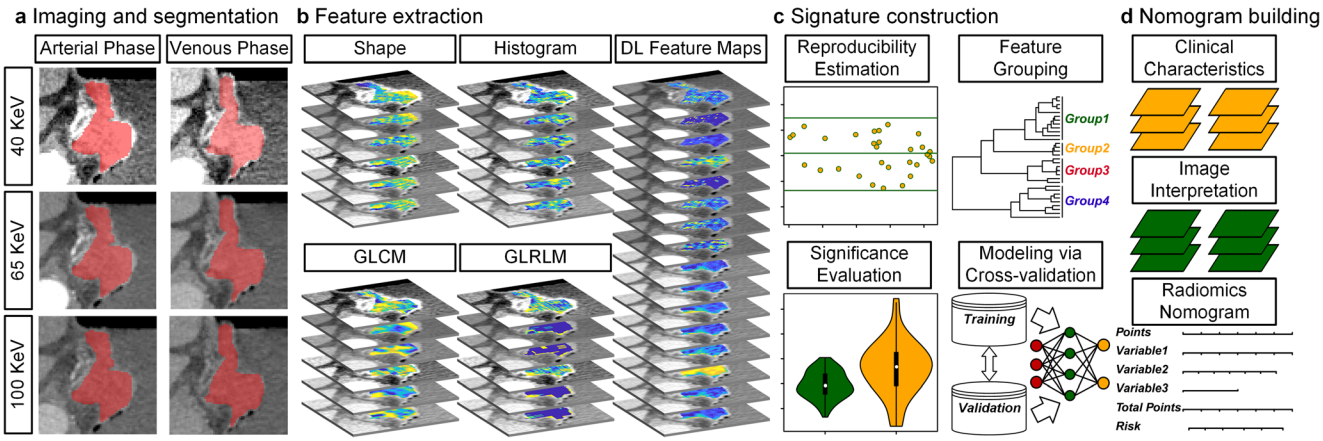

Fig. 2 Workflow of the dual-energy CT–based radiomics nomogram

Table 1 Characteristics of patients in training and test sets

Parameters		Training set				Test set			
		Overall	LNM(−)	LNM(+)	*p* value	Overall	LNM(−)	LNM(+)	*p* value
Age (mean ± SD, years)		58.98 ± 11.65	59.48 ± 11.57	58.67 ± 11.75	0.627[a]	58.54 ± 10.79	57.27 ± 10.82	59.55 ± 10.80	0.373[a]
Sex	Woman	38	13	25	0.548[c]	19	8	11	0.835[c]
	Man	98	39	59		49	22	27	
Borrmann classification	I	43	20	23	0.064[d]	16	11	5	0.053[d]
	II	48	21	27		25	11	14	
	III	40	10	30		21	5	16	
	IV	4	0	4		6	3	3	
Location	Cardia/fundus	60	23	37	0.878[c]	26	9	17	0.586[c]
	Body	37	15	22		20	10	10	
	Antrum	31	12	19		19	10	9	
	≥ 2/3 stomach	8	2	6		3	1	2	
Tumor thickness (mean ± SD, mm)		18.54 ± 8.58	15.29 ± 7.02	20.55 ± 8.88	< 0.001*[a]	17.80 ± 8.90	16.73 ± 10.90	18.64 ± 6.98	0.049*[a]
ICAP (100 μg/ml)		53.58 ± 20.39	51.93 ± 20.35	54.59 ± 20.46	0.461[b]	49.67 ± 19.78	50.51 ± 19.14	49.02 ± 20.49	0.761[b]
ICVP (100 μg/ml)		73.63 ± 24.92	69.05 ± 24.30	76.44 ± 25.02	0.094[b]	76.56 ± 40.23	87.07 ± 49.90	68.09 ± 28.32	0.153[a]
nICAP		0.15 ± 0.06	0.15 ± 0.06	0.16 ± 0.06	0.404[a]	0.15 ± 0.07	0.14 ± 0.07	0.16 ± 0.08	0.305[a]
nICVP		0.49 ± 0.19	0.44 ± 0.17	0.51 ± 0.19	0.043*[a]	0.49 ± 0.16	0.48 ± 0.16	0.50 ± 0.16	0.488[a]
CT-reported LN	Negative	77	42	35	< 0.001*[c]	38	25	13	< 0.001*[c]
	Positive	59	10	49		30	5	25	

AP, arterial phase; *VP*, venous phase; *IC*, iodine concentration; *nIC*, normalized iodine concentration; *LNM*, lymph node metastasis; *CT-reported LN*, CT-reported lymph node status. [a] Mann-Whitney *U* test; [b] Independent *t* test (for normal distribution indicated by the Shapiro test); [c] Chi-square test; [d] Fisher's exact test (for small frequency)

*p value < 0.05

Radiomics signature construction and validation

After excluding the non-reproducible features and the redundant features, a total of 68 AP and 51 VP CT features remained. Based on the two feature sets, two radiomics signatures were constructed by using four types of models and compared through cross-validation in the training set. For AP CT, the highest cross-validation accuracy of 0.63 was yielded from radial basis function (RBF) kernel SVM with two deep features and two handcrafted features as input features. For VP CT, the best model was linear ANN with one deep feature and one handcrafted feature input, yielding a cross-validation accuracy of 0.68. The results of cross-validation are listed in Table S1. Therefore, the AP and VP CT signatures were built using these two models. The two radiomics signatures exhibited good performance for the discrimination of LNM status in the test set, with AUCs of 0.71 (95% CI, 0.59–0.84) for AP CT signature and 0.76 (95% CI, 0.64–0.87) for VP CT signature.

Development of radiomics nomogram and comparative experiments

Multivariable regression with backward elimination was used to analyze the two radiomics signatures, tumor thickness, nICVP, and CT-reported LN. The results demonstrated that the two radiomics signatures and CT-reported LN remained significant after adjustment for cofactors (Table 2). Subsequently, using the derived regression coefficients, a radiomics nomogram was built as a quantitative method for noninvasive LNM prediction (Fig. 3).

As shown in Fig. 4, the developed nomogram exerted a powerful predictive ability in both training and test sets with AUCs of 0.84 (95% CI, 0.77–0.90) and 0.82 (95% CI, 0.72–0.92), respectively, which were higher than single-energy model (incorporating CT-reported LN and single-energy VP signature, Table S2) and clinical model (incorporating tumor thickness and CT-reported LN, Table S3). To assess the possibility of overfitting, the DeLong test was employed on the ROC curves of radiomics nomogram. The results indicated that the AUCs between training set and test set were not significantly different ($p = 0.772$). Furthermore, by splitting the whole data set randomly five times, different training and test sets were established to construct and validate the predictive model. And there was no significant difference found between the resulted ROC curves (with AUCs ranging from 0.80 to 0.84 in the test sets), demonstrating the robust and consistent performance of our method.

The optimal cut-off value of the multivariable logistic regression equation was selected as 0.62 to maximize Youden's

Table 2 Risk factors in radiomics nomogram

Variable	β	Adjusted OR (95% CI)	p value
Intercept	− 4.66		< 0.001
AP signature (per 0.1 increase)	0.42	1.52(1.08–2.15)	0.017
VP signature (per 0.1 increase)	0.36	1.43(1.06–1.93)	0.021
CT-reported LN (1 vs 0)	1.26	3.53(1.42–8.77)	0.006

AP, arterial phase; *VP*, venous phase; *CT-reported LN*, CT-reported lymph node status. 1 = CT-reported lymph node metastasis positive, 0 = CT-reported lymph node metastasis negative

index on the training set. By using this cut-off value, the developed nomogram yielded high performances in the training set (accuracy = 0.77, 95% CI 0.69–0.84; sensitivity = 0.77; and specificity = 0.77) and in the test set (accuracy = 0.76, 95% CI 0.65–0.86; sensitivity = 0.74; and specificity = 0.80). The results of NRI revealed that radiomics nomogram exhibited significantly better performance than the clinical model (NRI = 0.22, $p = 0.037$) and single-energy model (NRI = 0.19, $p = 0.040$) in the test set.

Detailed description on stratified analysis is provided in Supplemental Material. The results showed the performance of radiomics nomogram was not affected by tumor location, sex, and age (DeLong test, $p > 0.05$) (Figure S4), suggesting its generality on different kinds of cases. In addition, the nomogram calibration curves demonstrated good agreement between observed and predicted outcomes in the two sets (Hosmer-Lemeshow test, $p = 0.335$ and 0.403) (Fig. 5).

Comparison between radiomics nomogram and CT-reported LN

To investigate the improvement of LNM detection of the proposed radiomics nomogram, we evaluated its predictive performance in all 204 patients and in the CT-reported LN-negative (cN0) subgroup ($n = 115$). In the whole set, the radiomics nomogram demonstrated the best discrimination ability with an AUC of 0.83 (95% CI, 0.78–0.89). The DeLong test showed that there were significant improvements in contrast to the CT-reported LN and the developed clinical model ($p < 0.05$), which yielded AUCs of 0.71 (95% CI, 0.65–0.77) and 0.77 (95% CI, 0.70–0.84), respectively. Meanwhile, the statistically significant differences were also determined in the results of NRI ($p < 0.05$). In the cN0 subgroup, 70.00% (21/30) LNM-positive patients (i.e., the false-negative cases of CT-reported LN) were successfully detected by our nomogram, while a total of 79 patients were diagnosed correctly. The patients with relatively high nomogram values had a significantly greater possibility of being LNM positive (Mann-Whitney U test, $p < 0.05$).

The interpretation of CT-reported LN is unstable and highly experience-dependent. We assessed its intra-/inter-reader agreement using the kappa test, based on the re-interpretation for the whole set, and found that there were only poor to moderate agreements (kappa values = 0.45 and 0.25). Correspondingly, combining CT-reported LN with the two radiomics signatures, the radiomics nomogram achieved good agreements with the kappa values of 0.75 and 0.68 respectively. Furthermore, the predictive performance was maintained as well, as it yielded AUCs of 0.84 (95% CI, 0.78–0.89) and 0.86 (95% CI, 0.81–0.91). At one extreme, when the interpretation of radiologist was ignored (i.e., CT-reported LN was set to negative), the proposed nomogram still showed good discrimination ability with an AUC of 0.79 (0.73–0.85).

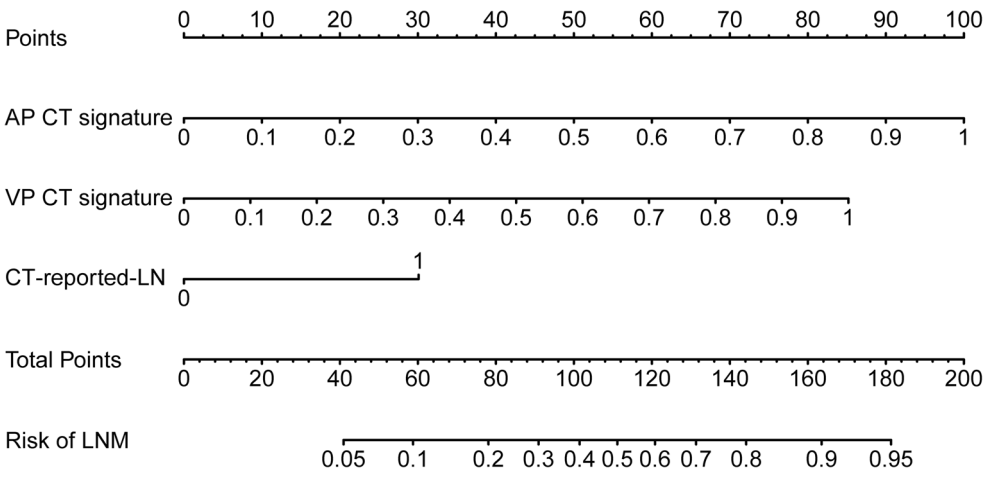

Fig. 3 Developed radiomics nomogram

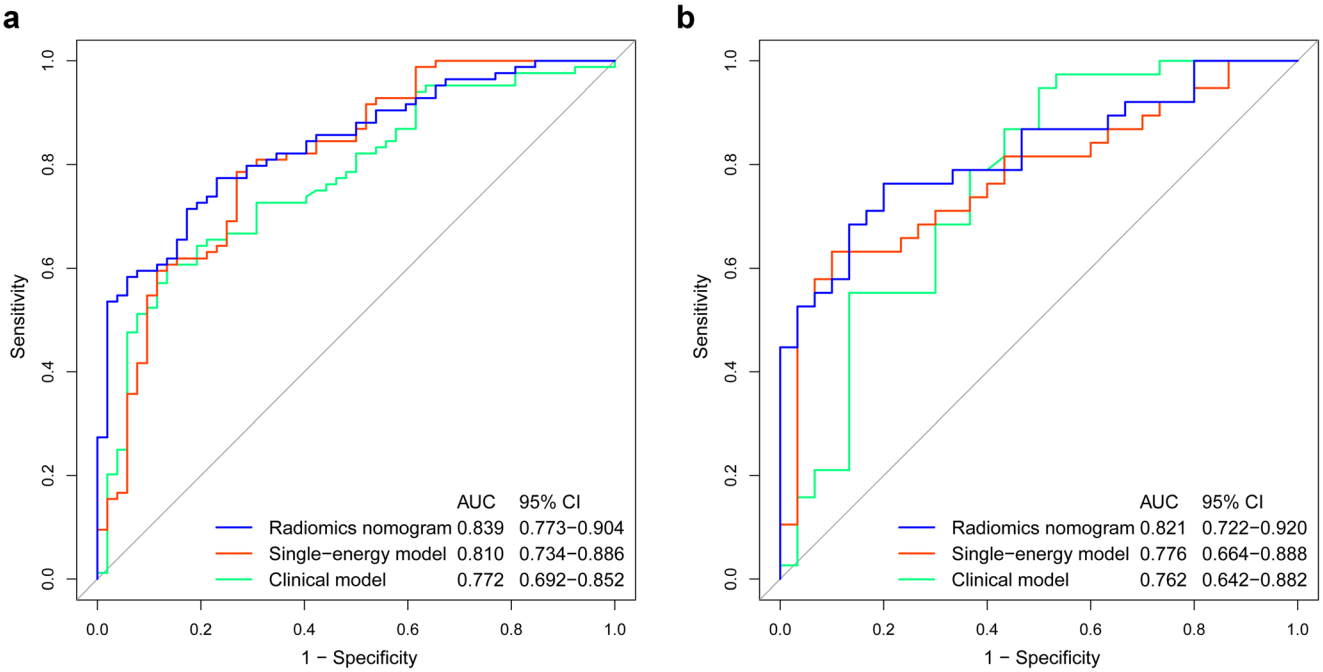

Fig. 4 Comparison of performances among the three developed models for the prediction of LNM in training set (**a**) and test set (**b**)

Prognostic value of radiomics nomogram

Based on the follow-up data, the prognostic value of the output score of our radiomics nomogram was assessed. It yielded high predictive accuracies for PFS (C-index = 0.64; 95% CI, 0.54–0.73; $p = 0.004$) and OS (C-index = 0.67; 95% CI, 0.56–0.78; $p = 0.002$). GC patients with elevated nomogram scores displayed worse PFS (HR = 1.22 per 0.1 increase, 95% CI

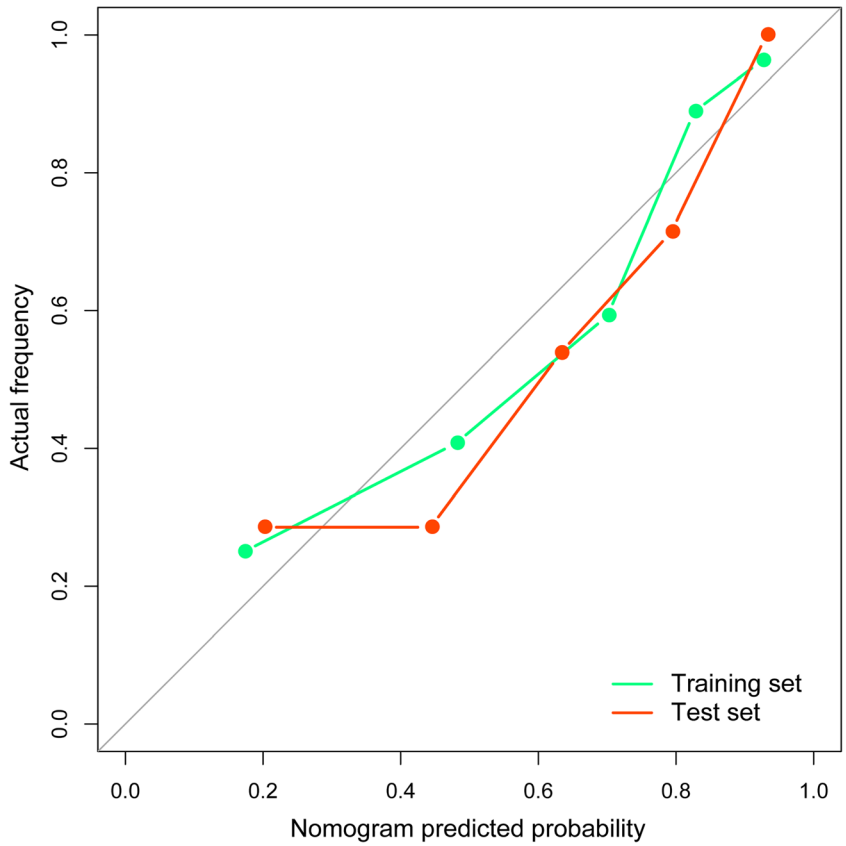

Fig. 5 Calibration curve of the radiomics nomogram in each set

1.04–1.43; $p = 0.015$) and OS (HR = 1.29 per 0.1 increase, 95% CI 1.06–1.58; $p = 0.012$).

Discussion

We have previously proved IC on dual-energy CT platform is an independent predictor of LNM in GC [27]. Hereby, we move forward to firstly build a dual-energy spectral CT imaging–based radiomics nomogram by deep learning method for LNM prediction in GC. According to the experimental results, the radiomics nomogram, which combined CT-reported lymph node status and two radiomics signatures, was clinically useful for the stratification of patients with GC according to LNM risk. And it performed better than single-energy model and clinical model.

The existing radiomics nomograms for the prediction of LNM used one-phase enhanced CT images [20, 21]. Instead, we used biphasic-enhanced images for feature extraction. Image acquisition of AP and VP phases were started around 30 s and 70 s following contrast agent administration. Typically, a linear enhancement in mucosa layer has been observed at AP, which reflects the functional capillary density in tissues [30]. GC with persistent enhancement has been identified at VP, indicating the process of iodine agent flows out from tumor tissues and diffuses into the interstitial spaces [14, 30]. Thus, the biphasic-enhanced images comprehensively characterized the vascularity of GC. Therefore, the incorporation of biphasic images into signature constructions can enrich radiomics analyses and improve the performance of the model. Plus, AP and VP radiomics signatures both presented significant association with LNM.

Dual-energy CT with energy information extends the capabilities of conventional CT, by providing iodine-water images for the quantification of actual iodine composition [31]. To date, only a few texture analyses have been performed on dual-energy CT [32, 33]. Al-Ajmi et al [32] found multi-energy image texture analysis demonstrates an improved accuracy (75% to 92%) for the diagnosis of parotid tumors compared with single-energy level of 65 keV. With respect to image selection for radiomics signature construction, 65 keV is relatively comparable to 120-kvp single-energy CT acquisition with higher contrast-to-noise ratio and less image noise [31, 34]. Based on CT physics and algorithms, low-energy images (40–70 keV) reflect tissue enhancement characteristics similar to the subtracted images, while high-energy images (100–140 keV) represent non-enhanced tissue features [32, 33] and we included the 40-keV image as representative for low-energy image. Referring to the plateau performance of spectral HU attenuation curve between 100 and 140 keV in Figure S1 (Supplementary Material), the 100-keV image was more visually comfortable and widely useful in clinical routine display thus was ultimately included. Compared with the single-energy model and clinical model, the multi-energy image-based radiomics nomogram demonstrated better performance and additional value from NRI test. Additionally, the combination of different energy images enriches the input features and increases the overall diagnostic accuracy for radiomics analysis.

The IC value reflects the actual iodine deposition in tissues [26, 35] and is considered a promising biomarker in gastric cancerous staging evaluation [26, 27, 36]. But we found the ICs were significant in univariable analysis and excluded during backward elimination and stepwise regression. We checked that there were only weak correlations between ICs and the three final retained indicators (Spearman's correlation coefficients < 0.2). This experimental result suggested that the two radiomics signatures, as well as the clinical indicator CT-reported-LN, yielded more apparent significance levels and therefore might be more influential. Besides, with regard to nIC, the values of aorta HU were relatively high in both AP and VP, which can lead to an inaccurate IC during the image thresholding steps.

Tumor size and CT-reported-LN were selected for model construction because they are easily accessible on the preoperative images. Tumor size and thickness play important roles in tumor staging and resectability as well as LNM. We found larger gastric tumors were identified with higher N staging, and tumor thickness was identified to be associated with LNM [14, 15]. These findings are consistent with previous studies [5, 14, 15, 27]. Tumor thickness was included in clinical model, but was removed from radiomics nomogram construction. Although CT yielded an unsatisfactory diagnostic accuracy (around 60%) for LNM determination, it is still comparable to other imaging modalities [13–15]. Considering the convenience and wide application of CT for LNM detection, CT-reported LN was included as a qualitative clinical feature for nomogram building and was significantly associated with LNM. Compared with CT-reported LN, our nomogram enables superior LNM prediction, especially for cN0 patients. The cN0 patients are classified as LNM-negative based on radiologist's experiences on CT images, whereas our nomogram showed promising performance to distinguish those who actually have greater LNM possibility in cN0 subgroup.

The limitation of this study is the lack of external validation for the developed nomogram, but we further randomly divided the patients into training set or test set and reconstructed and tested repeatedly five times to assess the results. And this pilot study is considered a pioneer to functional imaging radiomics analyses and gives us confidence to collaborate with other dual-energy CT centers for multicenter analyses. Our study placed two-dimensional freehand ROIs on the top three largest tumor slices for feature extraction, not the true three-dimensional volumes. We used representative energy level reference to literatures and practical experiences; whole spectrum of energy and truly volumetric analyses are expectable in the near future.

In conclusion, a noninvasive deep learning dual-energy CT–based radiomics nomogram was developed in this study. The proposed nomogram exhibited a favorable accuracy and added value for predicting LNM and prognosis in gastric cancer.

Funding information This study has received funding by National Natural Science Foundation of China (81271573, 91959130, 0, 81971776, 81771924).

Compliance with ethical standards

Guarantor The scientific guarantor of this publication is Jianbo Gao.

Conflict of interest The authors of this manuscript declare no relationships with any companies, whose products or services may be related to the subject matter of the article.

Statistics and biometry No complex statistical methods were necessary for this paper.

Informed consent Written informed consent was not required for this study because this is a retrospective diagnostic study. Written informed consent was waived by the Institutional Review Board of Zhengzhou University.

Ethical approval Institutional Review Board approval was obtained.

Study subjects or cohorts overlap A total of 73 of the 204 patients have been previously reported. This prior article dealt with the potential of IC value for the prediction of lymph node metastasis in gastric cancer by multivariate logistic analysis, whereas in this manuscript, we report on the additional predictive value of a deep learning spectral CT-based radiomics model for the LNM prediction in gastric cancer.

Methodology
- retrospective
- diagnostic or prognostic study
- performed at one institution

References

1. Ferlay J, Soerjomataram I, Dikshit R et al (2015) Cancer incidence and mortality worldwide: sources, methods and major patterns in GLOBOCAN 2012. Int J Cancer 136(5):E359–E386
2. GLOBOCAN (2012) Stomach cancer: estimated incidence, mortality and prevalence worldwide in 2012. Available at: http://globocan.iarc.fr/old/FactSheets/cancers/stomach-new.asp. Accessed 4 Nov 2014
3. Shen L, Shan YS, Hu HM et al (2013) Management of gastric cancer in Asia: resource-stratified guidelines. Lancet Oncol 14(12):e535–e547
4. Chen W, Zheng R, Baade PD et al (2016) Cancer statistics in China, 2015. CA Cancer J Clin 66(2):115–132
5. Saito H, Fukumoto Y, Osaki T et al (2007) Prognostic significance of level and number of lymph node metastases in patients with gastric cancer. Ann Surg Oncol 14(5):1688–1693
6. Oka S, Tanaka S, Kaneko I et al (2006) Advantage of endoscopic submucosal dissection compared with EMR for early gastric cancer. Gastrointest Endosc 64(6):877–883
7. Ajani JA, Bentrem DJ, Besh S et al (2013) Gastric cancer, version 2.2013: featured updates to the NCCN guidelines. J Natl Compr Canc Netw 11(5):531–546
8. Miyahara K, Hatta W, Nakagawa M et al (2018) The role of an undifferentiated component in submucosal invasion and submucosal invasion depth after endoscopic submucosal dissection for early gastric cancer. Digestion 98(3):161–168
9. Yamashita K, Hosoda K, Ema A, Watanabe M (2016) Lymph node ratio as a novel and simple prognostic factor in advanced gastric cancer. Eur J Surg Oncol 42(9):1253–1260
10. Persiani R, Rausei S, Biondi A, Boccia S, Cananzi F, D'Ugo D (2008) Ratio of metastatic lymph nodes: impact on staging and survival of gastric cancer. Eur J Surg Oncol 34(5):519–524
11. National Comprehensive Cancer Network (NCCN) guidelines. Available online: http://www.nccn.org/. Accessed on May 2018
12. Kwee RM, Kwee TC (2016) Imaging in local staging of gastric cancer: a systematic review. J Clin Oncol 25(15):2107–2116
13. Fairweather M, Jajoo K, Sainani N, Bertagnolli MM, Wang J (2015) Accuracy of EUS and CT imaging in preoperative gastric cancer staging. J Surg Oncol 111(8):1016–1020
14. Saito T, Kurokawa Y, Takiguchi S et al (2015) Accuracy of multidetector-row CT in diagnosing lymph node metastasis in patients with gastric cancer. Eur Radiol 25(2):368–374
15. Burbidge S, Mahady K, Naik K (2013) The role of CT and staging laparoscopy in the staging of gastric cancer. Clin Radiol 68(3):251–255
16. Limkin EJ, Sun R, Dercle L et al (2017) Promises and challenges for the implementation of computational medical imaging (radiomics) in oncology. Ann Oncol 28(6):1191–1206
17. Aerts HJ (2016) The potential of radiomic-based phenotyping in precision medicine: a review. JAMA Oncol 2(12):1636–1642
18. Lambin P, Leijenaar RTH, Deist TM et al (2017) Radiomics: the bridge between medical imaging and personalized medicine. Nat Rev Clin Oncol 14(12):749–762
19. Gillies RJ, Kinahan PE, Hricak H (2016) Radiomics: images are more than pictures, they are data. Radiology 278(2):563–577
20. Huang Y, Liang C, He L et al (2016) Development and validation of a radiomics nomogram for preoperative prediction of lymph node metastasis in colorectal cancer. J Clin Oncol 34(18):2157–2164
21. Wu S, Zheng J, Li Y et al (2017) A radiomics nomogram for the preoperative prediction of lymph node metastasis in bladder cancer. Clin Cancer Res 23(22):6904–6911
22. Jiang Y, Wang W, Chen C et al (2019) Radiomics signature on computed tomography imaging: association with lymph node metastasis in patients with gastric cancer. Front Oncol 9:340
23. Giganti F, Antunes S, Salerno A et al (2017) Gastric cancer: texture analysis from multidetector computed tomography as a potential preoperative prognostic biomarker. Eur Radiol 27(5):1831–1839
24. Liu S, He J, Liu S et al (2019) Radiomics analysis using contrast-enhanced CT for preoperative prediction of occult peritoneal metastasis in advanced gastric cancer. Eur Radiol. https://doi.org/10.1007/s00330-019-06368-5
25. Dong D, Tang L, Li Z et al (2019) Development and validation of an individualized nomogram to identify occult peritoneal metastasis in patients with advanced gastric cancer. Ann Oncol 30(3):431–438
26. Tang L, Li ZY, Li ZW et al (2015) Evaluating the response of gastric carcinomas to neoadjuvant chemotherapy using iodine concentration on spectral CT: a comparison with pathological regression. Clin Radiol 70(11):1198–1204
27. Li J, Fang M, Wang R et al (2018) Diagnostic accuracy of dual-energy CT-based nomograms to predict lymph node metastasis in gastric cancer. Eur Radiol 28(12):5241–5249
28. Lakhani P, Sundaram B (2017) Deep learning at chest radiography: automated classification of pulmonary tuberculosis by using convolutional neural networks. Radiology 284(2):574–582

29. Peng H, Dong D, Fang M et al (2019) Prognostic value of deep learning PET/CT-based radiomics: potential role for future individual induction chemotherapy in advanced nasopharyngeal carcinoma. Clin Cancer Res 25(14):4271–4279
30. Miles KA (1999) Tumour angiogenesis and its relation to contrast enhancement on computed tomography: a review. Eur J Radiol 30(3):198–205
31. Ogata T, Ueguchi T, Yagi M et al (2013) Feasibility and accuracy of relative electron density determined by virtual monochromatic CT value subtraction at two different energies using the gemstone spectral imaging. Radiat Oncol 8:83
32. Al Ajmi E, Forghani B, Reinhold C, Bayat M, Forghani R (2018) Spectral multi-energy CT texture analysis with machine learning for tissue classification: an investigation using classification of benign parotid tumours as a testing paradigm. Eur Radiol 28(6):2604–2611
33. Su KH, Kuo JW, Jordan DW et al (2018) Machine learning-based dual-energy CT parametric mapping. Phys Med Biol 63(12): 125001
34. Ozguner O, Dhanantwari A, Halliburton S, Wen G, Utrup S, Jordan D (2018) Objective image characterization of a spectral CT scanner with dual-layer detector. Phys Med Biol 63(2):025027
35. Jacobsen MC, Schellingerhout D, Wood CA et al (2018) Intermanufacturer comparison of dual-energy CT iodine quantification and monochromatic attenuation: a phantom study. Radiology 287(1):224–234
36. Pan Z, Pang L, Ding B et al (2013) Gastric cancer staging with dual energy spectral CT imaging. PLoS One 8(2):e53651